2013

Charge-Pairing Interactions Control The Conformational Setpoint and Motions of The FMN Domain in Neuronal Nitric Oxide Synthase

Mohammad Mahfuzul Haque
Lerner Research Institute

Mekki Bayachou
Cleveland State University, M.BAYACHOU@csuohio.edu

Mohammed A. Fadlalla
Lerner Research Institute

Deborah Durra
Lerner Research Institute

Dennis J. Stuehr
Cleveland State University, D.STUEHR@csuohio.edu

Charge-pairing interactions control the conformational setpoint and motions of the FMN domain in neuronal nitric oxide synthase

Mohammad Mahfuzul HAQUE , Mekki BAYACHOU , Mohammed A. FADLALLA , Deborah DURRA and Dennis J. STUEHR

The NOS (nitric oxide synthase; EC 1.14.13.39) enzymes contain a C-terminal flavoprotein domain [NOSred (reductase domain of NOS)] that binds FAD and FMN, and an N-terminal oxygenase domain that binds haem. Evidence suggests that the FMN-binding domain undergoes large conformational motions to shuttle electrons between the NADPH/FAD-binding domain [FNR (ferredoxin NADP-reductase)] and the oxygenase domain. Previously we have shown that three residues on the FMN domain (Glu^{762}, Glu^{816} and Glu^{819}) that make charge-pairing interactions with the FNR help to slow electron flux through nNOSred (neuronal NOSred). In the present study, we show that charge neutralization or reversal at each of these residues alters the setpoint [K_{eq}(A)] of the NOSred conformational equilibrium to favour the open (FMN-deshielded) conformational state. Moreover, computer simulations of the kinetic traces of cytochrome *c* reduction by the mutants suggest that they have higher conformational transition rates (1.5–4-fold) and rates of interflavin electron transfer (1.5–2-fold) relative to wild-type nNOSred. We conclude that the three charge-pairing residues on the FMN domain govern electron flux through nNOSred by stabilizing its closed (FMN-shielded) conformational state and by retarding the rate of conformational switching between its open and closed conformations.

Key words: conformational equilibrium, domain motion, electron flux, flavoprotein, electron transfer, neuronal nitric oxide synthase (nNOS).

INTRODUCTION

NO (nitric oxide) is involved in cardiovascular, neuronal and immune functions during both normal and disease states [1,2]. NO is produced in mammals by three isoforms of NOS (nitric oxide synthase; EC 1.14.13.39) known as nNOS (neuronal NOS), eNOS (endothelial NOS) and iNOS (inducible NOS). All three are homodimeric enzymes that catalyse a two-step oxidation of L-Arg (L-arginine) to generate NO and citrulline [3]. They are comprised of an N-terminal oxygenase domain (NOSoxy) that contains binding sites for iron protoporphyrin IX (haem), H_4B [(6*R*)-5,6,7,8-tetrahydro-L-biopterin] and L-Arg, a C-terminal reductase domain [NOSred (reductase domain of NOS)] that contains binding sites for FAD, FMN and NADPH, and an intervening CaM (calmodulin)-binding sequence [4]. The NOSoxy, NOSred and CaM-binding domains can be expressed independently and have been subject to detailed structural, kinetic and regulatory studies [5–9].

NOSred shares structural and catalytic features with a family of dual flavin enzymes, including NADPH CPR (cytochrome P450 reductase), the flavoprotein of *Escherichia coli* sulfite reductase, methionine synthase reductase, novel reductase-1 and the reductase domain of bacterial cytochrome P450BM3 [10–14]. These proteins are comprised of separate FMN-binding and FAD/NADPH-binding [FNR (ferredoxin NADP-reductase)] domains that are attached by a flexible hinge [6,15]. During catalysis, the FAD receives a hydride from NADPH and then sequentially passes electrons to the FMN cofactor. Ultimately, the 2-electron reduced FMN hydroquinone transfers an electron to a haem group in a separate acceptor enzyme, or in the case of NOS, to the haem located in the NOSoxy domain of the partner subunit of the dimer [16,17]. The FMN hydroquinone in these enzymes can also reduce external electron acceptors such as cytochrome *c* [18] and this activity is widely used as a tool to study electron flux through NOSred and related enzymes.

The FMN domain in the dual flavin reductases is thought to undergo relatively large conformational motions in order to transfer electrons during catalysis [6,8,11,13,19–22]. Figure 1 illustrates a model for FMN domain conformational switching during electron transfer within a NOS homodimer. The FMN domain must first interact with the FNR domain in a 'FMN-shielded' conformation to receive electrons, according to equilibrium A. Once the FMN hydroquinone ($FMNH_2$) forms, it must swing away to a 'FMN-deshielded' conformation, and then must interact with the NOSoxy domain in the partner subunit of a NOS dimer, according to equilibrium B. Its interaction with the NOSoxy domain allows the FMN-to-haem electron transfer [8]. Data suggest that conformational equilibria A and B have their own intrinsic set points (K_{eq}) and individual control [8,20], and that the FMN-to-haem electron transfer step is fast once a productive docking conformation is achieved [23], which implies that the conformational kinetic parameters may be rate-limiting for the entire process.

The reductase activities of nNOSred and eNOSred are, with the exception of novel reductase-1 [11], repressed when compared with the other family members, but CaM binding to the NOS enzymes relieves this repression. The CaM effect is associated with its shifting equilibrium A toward the FMN-deshielded state in nNOSred and eNOSred [7,8,19,20,24,25]. This forms the basis for the hypothesis that electron flux is regulated by

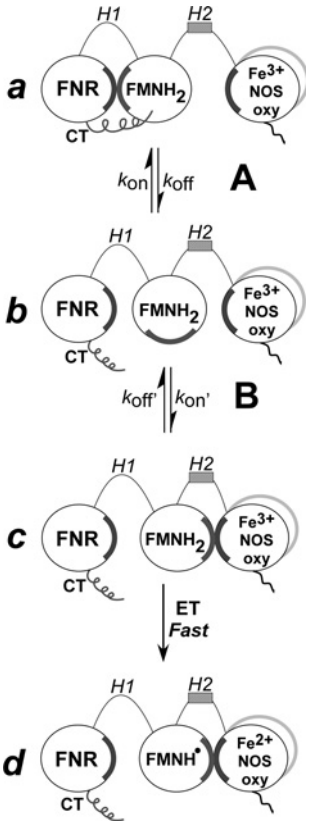

Figure 1 Model of NOS FMN domain function in electron transfer and haem reduction

Electron transfer in NOS is mainly regulated by two conformational equilibria, A and B. Equilibrium A indicates the change between a conformation in which FNR and FMN domains are interacting (**a**) and a conformation where the FMN domain is deshielded and available for interaction with electron acceptors such as cytochrome *c* (**b**). Note that the CT stabilizes conformation (**a**). Equilibrium B indicates the transition from the FMN-deshielded conformation (**b**) to a FMN-NOSoxy domain interacting state (**c**). Once the FMN and the oxygenase domains are close, electron transfer to the haem is fast (**d**). ET, electron transfer; FMNH•, FMNsq.

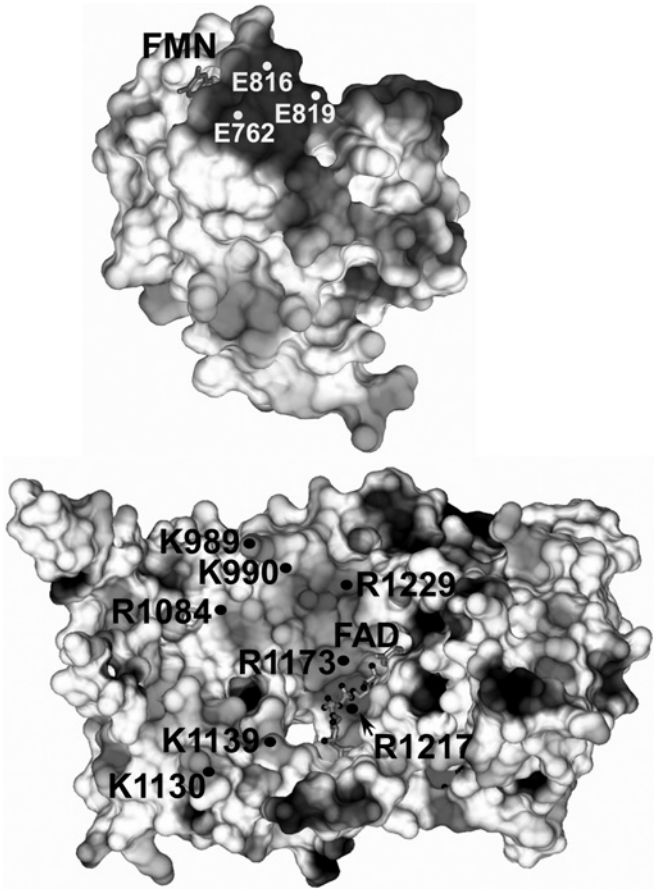

Figure 2 Structure of the nNOS FMN and FNR domains

FMN domain showing the location of Glu^{762}, Glu^{816} and Glu^{819} residues (upper panel). The interacting surface of the FNR module contains an electropositive patch (lower panel). Amino acids are in single letter code. Black, negatively charged surface; light grey, positively charged surface.

conformational parameters, namely the setpoint and transition rates of conformational equilibrium A [24,26]. In CaM-free NOS, the FMN-shielded conformation is relatively stable and a crystal structure of nNOSred in this putative conformation is available [6]. We know that electron flux through NOSred is regulated by several unique structural elements that include an AI (autoinhibitory insert) sequence within the FMN domain [7,27,28], a CT (C-terminal tail) [9,25,29,30], phosphorylation sites [31–33], a loop within the connecting domain [34], which may act in concert with other structural features that NOS shares with dual-flavin reductases, such as the FMN–FNR domain connecting hinge [35], a conserved aromatic residue (Phe^{1395} in nNOS) that stacks against the FAD isoalloxazine ring and governs the NADPH nicotinamide interaction [24,36], surface residues that form charge-pairing interactions between the FMN and FNR domains [37–39], and NADP(H) binding [19,25]. So far, the CT, AI, Phe^{1395} and NADPH-binding interaction have all been shown to stabilize the FMN-shielded state of CaM-free nNOSred [7,9,19,24]. In the present study we investigate the mechanism by which complementary charge-pairing interactions at the FMN–FNR domain interface influence electron flux through nNOS, specifically testing if they do so by impacting the conformational parameters of equilibrium A. In our previous study [38], we surveyed six electronegative surface residues on the FMN domain that form charge-pairing interactions with the FNR domain, and identified three that have the greatest capacity to slow electron flux through nNOSred (Glu^{762}, Glu^{816} and Glu^{819}) (Figure 2). The present study shows that charge neutralization or reversal at each of these sites alters both the setpoint and transition rates of equilibrium A, and that these changes can fully explain the increased electron flux seen in the mutants. Thus we provide the first experimental evidence that interdomain charge-pairing interactions influence electron flux primarily by tuning the conformational parameters of the FMN domain during catalysis.

EXPERIMENTAL

General methods and materials

All reagents and materials were obtained from Sigma, Amersham Biosciences or other sources as reported previously [7,20,24,37]. Absorption spectra and steady-state kinetic data were obtained using a Shimadzu UV-2401PC spectrophotometer. Single wavelength stopped-flow kinetic experiments were performed using a Hi-Tech Scientific SF-61 instrument equipped with anaerobic setup and photomultiplier detection. Data from multiple identical stopped-flow experiments were averaged to improve the signal-to-noise ratio. The spectral traces were fitted according to single or multiple exponential equations using software provided

by the instrument manufacturer. The best fit was determined when adding further exponentials did not improve the fit as judged from the residuals. All plots and additional curve fitting were done using Origin 8.0 (OriginLab). All experiments were repeated two or more times with at least two independently prepared batches of proteins to ensure consistent reproducibility of the results. The results were analysed and are expressed as means $\pm$ S.D. For all experiments and protein purifications, the buffer used contained 40 mM EPPS [4-(2-hydroxyethyl)-1-piperazinepropanesulfonic acid] (pH 7.6), 10 % (v/v) glycerol and 150 mM NaCl, unless noted otherwise. Anaerobic samples were prepared in an air-tight cuvette using repeated cycles of vacuum followed by a positive pressure of catalyst-deoxygenated nitrogen gas. All nNOSred proteins samples were fully oxidized by adding potassium ferricyanide, and the excess potassium ferricyanide was removed by passing through a Sephadex G-25 column (PD-10, GE Healthcare).

Generation of nNOSred mutants

The bacterial expression vector pCWori contained cDNA that coded for rat nNOSred with its adjacent N-terminal CaM-binding motif (Met^{695}–Ser^{1429}) as described previously [24]. Oligonucleotides for site-directed mutagenesis were obtained from Integrated DNA Technologies and are listed in Supplementary Table S1 (at http://www.biochemj.org/bj/450/bj4500607add.htm). Site-directed mutagenesis was performed using the QuikChange® XL mutagenesis kit (Agilent Technologies-Stratagene). Mutations were confirmed by DNA sequencing at the Cleveland Clinic Genomics Core Facility. Mutated plasmids were transformed into *E. coli* BL21(DE3) cells transformed with a pACYC plasmid containing human CaM to co-express CaM with the protein.

Expression and purification of WT (wild-type) and mutant nNOSred proteins

WT and mutant enzyme expression was induced at room temperature (25 °C) over 1 or 2 days in *E. coli* BL21(DE3) that harboured the pACYC-CaM plasmid as described previously [24]. The nNOSred proteins were purified by sequential chromatography on a 2′,5′-ADP–Sepharose affinity column and CaM–Sepharose resin as reported previously [24]. The purity of each protein was assessed by SDS/PAGE and spectral analysis. For the nNOSred proteins, the concentration was determined by using a molar absorption coefficient of 22 900 $M^{-1}\cdot cm^{-1}$ at 457 nm for the fully oxidized form [40].

Steady-state cytochrome *c* reduction assays

The cytochrome *c* reductase activity was determined at 25 °C and 10 °C by monitoring the absorbance increase at 550 nm and using an molar absorption coefficient $\varepsilon_{550} = 21\ mM^{-1}\cdot cm^{-1}$ as described previously [7,24,25,41].

Oxidation of reduced nNOSred proteins

A solution of fully oxidized nNOSred protein (6–8 μM) containing either EDTA (1 mM) or $CaCl_2$ (2 mM) plus CaM (30–40 μM) in air-saturated buffer was reduced by adding NADPH (120–160 μM) and then allowed to auto-oxidize at room temperature in an open cuvette [24,25]. The process was monitored at 457 nm, and visible spectra at the indicated time points (see the Results section) were recorded in similar experiments.

Anaerobic stopped-flow flavin reduction kinetics in nNOSred proteins

The absorbance changes associated with nNOSred flavin reduction by NADPH were recorded by rapidly mixing a solution of oxidized nNOSred (8–10 μM) containing either EDTA (1 mM) or $CaCl_2$ (2 mM) plus CaM (80–100 μM) with a solution of approximately 100 μM NADPH at 10 °C in the stopped-flow instrument. The maximum absorbance value for a given protein sample at 457 nm during single wavelength experiments was obtained by replacing the NADPH solution in one of the stopped-flow syringes with buffer only and recording additional mixing events. The individual rate constants associated with absorbance changes at 457 nm were first estimated by analysis of experiments of various lengths. The final reported values were obtained by fitting an experiment on a timescale capturing all three rate constants to a triple exponential function, such that the residuals were minimized and contained little or no systematic deviation between the fit curve and the actual data. Percentage absorbance changes were calculated on the basis of the absorbance change in the instrument dead time and the relative proportions of the ΔA values for each kinetic phase obtained from the fitting program [7,24].

Reaction of fully reduced nNOSred proteins with excess cytochrome *c*

The rate of reduction of excess cytochrome *c* by fully reduced nNOSred proteins was measured in the stopped-flow instrument under anaerobic conditions at 10 °C as described previously [20]. The nNOSred (10–15 μM) protein in 40 mM EPPS buffer (pH 7.6) with 10 % (v/v) glycerol and 150 mM NaCl containing EDTA (2 mM) was fully reduced by titrating it with anaerobic sodium dithionite solution. A solution of fully reduced nNOSred proteins containing NADPH (200 μM) was mixed with cytochrome *c* (100 μM) while monitoring the absorbance changes at 550 nm. We have also measured the rate of cytochrome *c* reduction by photo-reduced nNOSred proteins under various conditions in the stopped-flow apparatus. Briefly, each nNOSred protein (10–15 μM), 5-deazariboflavin ($\sim$1 μM) and EDTA (1 mM) was completely photo-reduced in an anaerobic cuvette using a commercial slide projector bulb until no changes in the UV–visible spectrum of the sample were observed upon further irradiation of the sample. The fully reduced protein sample was rapidly mixed in the stopped-flow instrument with a solution of cytochrome *c* ($\sim$100 μM) at 10 °C. The absorbance change at 550 nm was recorded. In a second set of experiments, 1 mM NADPH was added to the photo-reduced protein sample, and the mixture was incubated at 10 °C for 15 min and scanned to confirm the protein remained fully reduced prior to mixing. Multiple absorbance traces were averaged and fitted to a single or double exponential function. Initially, a solution of cytochrome *c* and NADPH was mixed with anaerobic buffer to obtain the initial absorbance reading at zero time in both dithionite-reduced and photoreduced enzymes. A linear regression analysis of late points in the traces and/or numeric derivatives of the traces were run to determine the deflection points separating the early burst of fast-reacting and late slow-reacting phases (see the Results section).

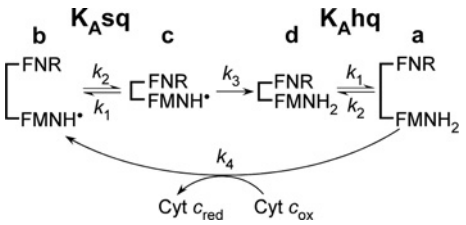

Figure 3 Kinetic model for electron flux through a dual-flavin enzyme

The model uses four kinetic rates: association (k_1 or k_3) and dissociation (k_{-1} or k_{-3}) of the FMN and FNR domains; the FMNsq (FMNH•) reduction rate (k_2), and the cytochrome *c* reduction rate (k_4). The fully reduced enzyme in the open conformation (species a) reduces cytochrome *c* and generates species b, which then undergoes successive conformational closing, interflavin electron transfer and conformational opening steps to complete the cycle. Cyt *c*, cytochrome *c*; hq, hydroquinone; ox, oxidized; red, reduced; sq, semiquinone.

Simulation of the kinetic traces of fully reduced nNOSred proteins with excess cytochrome *c*

We used the computer program Gepasi v.3.30 [42] to simulate the experimental electron flux to cytochrome *c* using the kinetic model as outlined in Figure 3. Details of this type of simulation have been reported recently [43]. Briefly, cytochrome *c* was set to be in 100-fold molar excess relative to the various flavoproteins and each simulation was started with 100 % of the enzyme in the fully reduced state. Input rates (k_1, k_{-1}, k_3 and k_{-3}) that satisfy the observed conformational equilibrium constant are first used, and then refined in an iterative process using the time of first turnover and overall best fit of the kinetic trace as criteria to extract the best rates for FMN conformational motion and interflavin electron transfer.

RESULTS

Cytochrome *c* reductase activity in the absence and presence of bound CaM

The cytochrome *c* reductase activity of nNOSred is repressed in the native state and the repression is relieved upon CaM binding [44]. We examined how the FMN domain surface mutations would impact nNOSred reductase activities in the CaM-free or CaM-bound states (Figure 4A and Supplementary Table S2 at http://www.biochemj.org/bj/450/bj4500607add.htm). All assays contained SOD (superoxide dismutase) to insure we only detected reductase activity that involved a direct electron transfer from nNOSred to cytochrome *c* [18,19]. The CaM-free E762N, E762R, E816R, E819R and triple mutant (E762R/E816R/E819R) displayed activities at 25 °C that were ~9.9-fold, ~8.7-fold, 5.1-fold, 4-fold and 8.9-fold greater than CaM-free WT nNOSred respectively. Similar results were obtained when we ran the assays at 10 °C (Figure 4B). CaM enhanced the nNOSred reductase activity approximately 9-fold, but caused smaller increases in E816R and E819R or had a negligible effect in E762N, E762R and triple mutant, consistent with their higher CaM-free reductase activities. These results suggest that the charge pairings normally help repress electron flux through the CaM-free protein, but have little impact on electron flux once CaM is bound.

Flavin auto-oxidation

We next determined whether the mutations altered the flavin auto-oxidation rate or the air stability of the FMNsq (FMN semiquinone). We mixed each fully oxidized protein with a 20-fold molar excess of NADPH in air-saturated buffer and

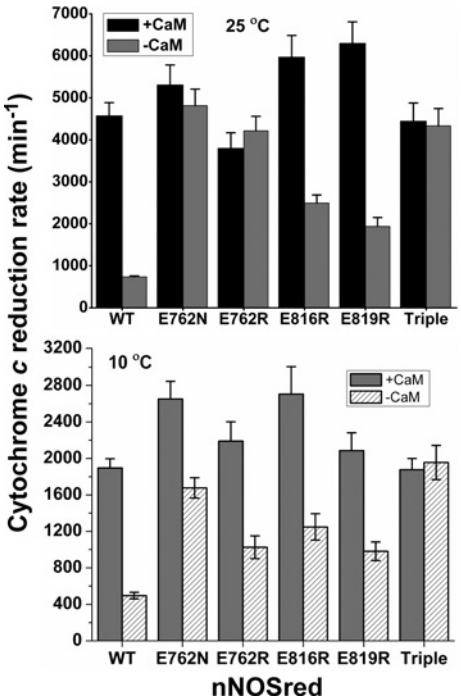

Figure 4 Steady-state cytochrome *c* reductase activities of nNOS and mutants in the absence and presence of CaM

Activities were measured at 25 °C and at 10 °C in the presence of SOD and either in the absence or presence of CaM. Values are representative of three measurements done under identical conditions, using two different protein preparations for each mutant. Error bars are ± S.D.

followed changes in the flavin reduction status at 457 nm against time, and also collected visible spectra prior to NADPH addition, during steady-state NADPH oxidation, and after all the NADPH had been oxidized (Figure 5 and Supplementary Figure S1 at http://www.biochemj.org/bj/450/bj4500607add.htm). After NADPH addition, all proteins achieved a similar level of flavin reduction in the steady state and all showed a prominent flavin semiquinone absorbance at 600 nm. However, the E819R, E762R, triple mutant, E762N and E816R nNOSred mutants consumed NADPH at rates approximately 1.1-, 1.6-, 1.7-, 1.9- and 2.0-fold higher than WT nNOSred respectively. All mutants except E819R also exhibited 2–3.5-fold higher rates of flavin re-oxidation after the NADPH was depleted (Figures 5A and 5B, and Supplementary Figure S1). An inspection of the final absorbance traces and the final absorbance values at 457 nm indicate that all the proteins except for the E762R and the triple mutant were left with an air-stable FMNsq as occurs in WT nNOSred [24,45]. This is consistent with our observation that these mutants purify as fully oxidized proteins (bright yellow with an absence of FMNsq absorbance). Thus most of the mutations increased flavin auto-oxidation rates and, in some cases, diminished the air stability of the FMNsq radical.

Kinetics of flavin reduction in fully oxidized nNOSred enzymes

We next examined the flavin reduction kinetics in the mutant proteins. The reactions mixed the fully oxidized nNOSred proteins with excess NADPH at 10 °C under anaerobic conditions in a single-wavelength stopped-flow spectrophotometer, and flavin reduction was followed at 457 nm. All traces fitted well to a triple exponential equation [7,46]. The results are listed in Table 1, and fits are shown in Supplementary Figure S2

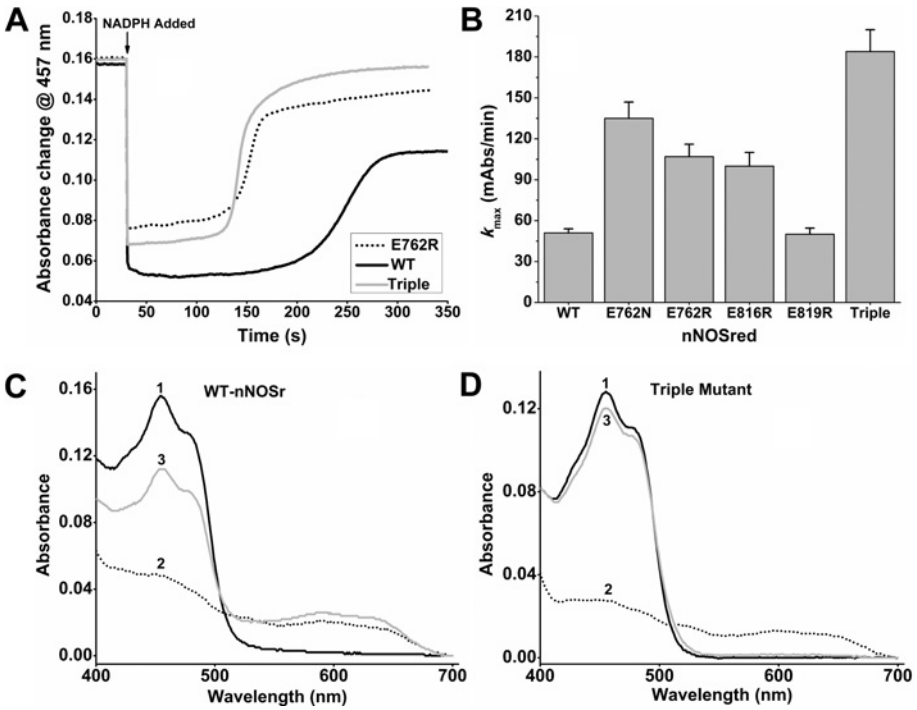

Figure 5 Kinetics of flavin auto-oxidation in the NADPH-reduced WT and mutant nNOSred enzymes

WT and mutant nNOSred proteins were diluted to ~6 μM in air-saturated buffer in a cuvette, given a 15-fold molar excess of NADPH, and then allowed to consume NADPH at room temperature as described in the Experimental section. (**A**) The redox status of enzyme flavins was monitored at 457 nm over time. (**B**) Flavin auto-oxidation rates (mAbs/min). Error bars are + S.D. (**C** and **D**) The visible spectra shown were recorded for the WT and triple mutant (E762R/E816R/E819R) nNOSred prior to NADPH addition (trace 1), during NADPH consumption (trace 2), and after all the NADPH had been consumed and flavin reoxidation had occurred (trace 3). The results are representative of two independent experiments.

Table 1 Rates of NADPH-dependent flavin reduction of nNOSred proteins

Reactions were carried out in a stopped-flow instrument at 10 °C by mixing oxidized enzymes with a 10-fold molar excess of NADPH and monitoring the absorbance changes at 457 nm. The results were fitted to a triple exponential function as described in the Experimental section. Values are the means ± S.D. for at least two trials and representative of data obtained with two preparations.

nNOSred	Conditions	Dead time (%)	k_1 (s^{-1})† (%)	k_2 (s^{-1})† (%)	k_3 (s^{-1})† (%)
WT	−CaM	18	59 ± 7 (28)	4.4 ± 0.3 (31)	0.86 ± 0.02 (23)
	+CaM	23	159 ± 4 (37)	18.5 ± 0.5 (29)	1.8 ± 0.2 (11)
E762N	−CaM	25	129 ± 6 (32)	11 ± 1 (18)	2.3 ± 0.1 (25)
	+CaM	26	146 ± 3 (48)	14.5 ± 1.8 (11)	2.5 ± 0.2 (15)
E762R	−CaM	17	113 ± 7 (35)	4.4 ± 0.5 (21.5)	0.8 ± 0.1 (26.5)
	+CaM	24	130 ± 9 (38.5)	6.0 ± 0.5 (12)	1.3 ± 0.1 (25.5)
E816R	−CaM	16	178 ± 12 (27)	9.0 ± 0.3 (34)	1.1 ± 0.1 (23)
	+CaM	19	214 ± 17 (32)	10.7 ± 1 (33)	1.0 ± 0.1 (16)
E819R	−CaM	14	82 ± 6 (28)	7.0 ± 0.8 (27.5)	1.5 ± 0.1 (30.5)
	+CaM	15	119 ± 6 (25)	18.0 ± 1.2 (31)	2.7 ± 0.1 (29)
Triple mutant	−CaM	15	163 ± 13 (28)	9.1 ± 0.4 (43.5)	0.95 ± 0.1 (13.5)
	+CaM	15	211 ± 19 (32)	11 ± 1 (46)	1.43 ± 0.18 (7)

*Percentage of the total absorbance change occurring in the instrument dead time.
†Values are the calculated rates with% of the total absorbance change attributed to that phase in parenthesis.

(at http://www.biochemj.org/bj/450/bj4500607add.htm). A significant proportion (15–25 %) of the total absorbance decrease at 457 nm occurred in the mixing dead time in all cases, consistent with previous reports [7,24,25]. At 457 nm, the initial phase is considered to reflect the hydride transfer from NADPH to FAD, followed by slower phases that reflect interflavin electron transfer, $NADP^+$ dissociation, and further reduction by a second NADPH [22]. All the mutants displayed higher flavin reduction kinetics in their CaM-free state relative to WT nNOSred. The magnitudes of their rate increases generally correlated with the degree to which their cytochrome *c* reductase activities had increased (Figure 4). The flavin reduction kinetics in CaM-free E762N, E762R, E816R and the triple mutant were increased enough (Table 1) to approach the rates observed for CaM-bound WT nNOSred, whereas the CaM-free E819R mutant had an intermediate behaviour that was closer to WT. Thus most mutants lost most or all of the kinetic repression on flavin reduction that is normally present in CaM-free nNOSred [24,45].

Conformational equilibrium of nNOSred

In nNOSred the FMN domain shifts between shielded and deshielded conformational states [25,26,36,40] and only the deshielded state is capable of transferring electrons to cytochrome

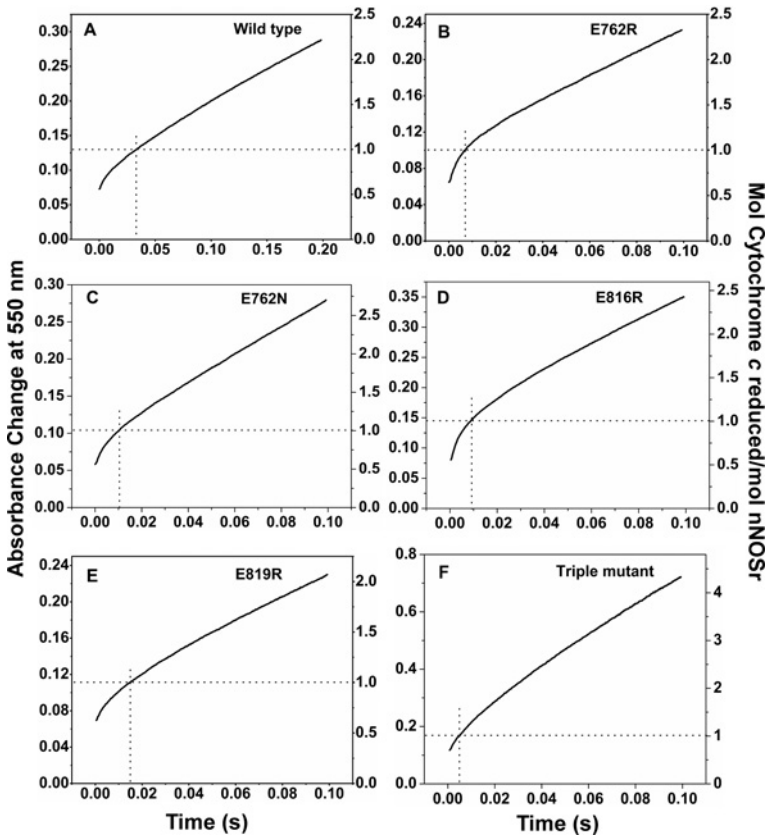

Figure 6 Reaction of fully reduced WT and mutant nNOSred proteins with excess cytochrome *c*

Solutions of pre-reduced, CaM-free nNOSred (6–10 μM) containing 200 μM NADPH were rapidly mixed with cytochrome *c* (100 μM) in a stopped-flow instrument under anaerobic conditions at 10 °C. Kinetic traces were recorded at 550 nm during the first few electron transfers to cytochrome *c*. The absorbance change representing the first turnover is shown by broken lines according to the right-hand scale in each Figure. The results are representative of at least two experiments.

c. This makes the cytochrome *c* reductase activity of nNOSred sensitive to the degree of FMN shielding and to the associated transition rates between the open and closed conformational states [8,9,20,24,26]. One way to study the conformational equilibrium is by a stopped-flow spectroscopic method that monitors the reaction of fully reduced enzyme with a large molar excess of cytochrome *c*. Under this circumstance, the kinetics of the absorbance change that occurs during reduction of the first few molar equivalents of cytochrome *c* can provide the K_{eq}(A) setpoint for the conformational equilibrium, and through computer modelling of the absorbance trace using the kinetic model in Figure 3, in most cases can provide rate estimates for the conformational transitions between the FMN-shielded and -deshielded forms [20,43].

We rapidly mixed the NADPH-bound forms of each fully reduced (dithionite) nNOSred protein with a 10-fold excess of cytochrome *c* in the stopped-flow spectrometer at 10 °C, and monitored the first few turnovers of cytochrome *c* reduction at 550 nm. Representative kinetic traces obtained for WT nNOSred and each mutant protein are shown in Figure 6. The starting absorbance values at zero time were determined in each case by mixing enzyme-free buffer with cytochrome *c* under otherwise identical conditions. Upon mixing each reduced enzyme with excess cytochrome *c*, there was a rapid absorbance increase that took place in the mixing dead time followed by a slower observable absorbance increase. In the case of the WT nNOSred, approximately 50 % of the total absorbance change that is ascribed to reduction of the first equivalent of cytochrome *c* (the portion of the trace confined within the dashed boxes in each panel of Figure 6) occurred within the mixing dead time, and the remaining 50 % occurred during the subsequent observable period (Figure 6A). This indicates that equivalent amounts of FMN-shielded and -deshielded enzyme conformers were present at the time of mixing, giving an estimated K_{eq}(A) value of 1 for the conformational equilibrium of CaM-free fully reduced NADPH-bound WT nNOSred, consistent with our previous estimate [20]. In comparison, the mutants had either similar or somewhat larger portions of their first turnovers completed within the mixing dead time (Figures 6B–6F), indicating that they have somewhat higher K_{eq}(A) values for their conformational equilibrium compared with WT, and thus slightly favour the FMN-deshielded conformer. The calculated K_{eq}(A) values of the NADPH-bound enzymes are listed in Table 2. The rates of cytochrome *c* reduction subsequent to transfer of the first electron equivalent (i.e. slope of line after the dashed box) were all considerably higher in the mutants than in WT nNOSred, consistent with the mutants with higher steady-state reductase activities. Thus the results indicate that the conformational equilibrium setpoints of the fully reduced NADPH-bound mutants are slightly altered to favour the FMN-deshielded state, according to the following rank order of highest to lowest K_{eq}(A): triple mutant>E819R>E762R>E762N>E816R>WT (Table 2).

Table 2 Kinetic parameters for WT nNOSred and mutants derived from experimental traces of cytochrome *c* reduction or from fitting the experimental traces according to the four-state kinetic model

Data are representative of two to three trials with each protein. Values in parentheses are experimental values. ND, not determined.

nNOSred	Measured K_A	Best fit $k_1 = k_3$ (s^{-1})	Best fit $k_{-1} = k_{-3}$ (s^{-1})	Best fit k_2 (s^{-1})	Fitted steady-state electron flux (s^{-1})	Fitted time elapsed for first turnover (ms)
WT	1	60	60	20	7.6 (7.6)	34 (31)
E762R	1.53	150	230	38	12.9 (11.8)	9.5 (9.5)
E762N	1.32	150	198	55	18.55 (17.9)	10.8 (10.8)
E816R	1.25	200	250	41	15.6 (14.3)	9.0 (8.8)
E819R	1.63	80	130	42	11.65 (11.46)	15 (16.5)
Triple	2.33	–	–	–	ND (31.1)	ND (5.3)

Effect of bound NADPH on conformational behaviours

This stopped-flow approach can be utilized to determine how bound NADPH impacts the conformational equilibrium, and whether the mutations alter this aspect. Bound NADPH has been reported to stabilize the FMN-shielded or closed conformation of nNOSred [9,19,25]. In the present study we investigated this by comparing the behaviour of the enzymes after they had been fully photoreduced with either the addition of NADPH, or not. The kinetic traces in Figures 7(A) and 7(B) show that the fully photoreduced WT nNOSred exists in an approximate 50:50 mix of open and closed conformers in both its NADPH-free and -bound states. This indicates that bound NADPH has little or no influence on the K_{eq}(A) setpoint of the fully reduced WT nNOSred, which differs from previous studies. However, these same two traces show that bound NADPH did greatly slow the transfer of the remainder of the first electron equivalent to cytochrome *c* (compare the slopes of the traces within the dashed boxes) and also slowed subsequent transfer of the second electron equivalent out of nNOSred. In comparison, traces recorded for three of the mutants in their NADPH-free states (Figures 7C, 7E and 7G) show that the first electron equivalent is almost entirely transferred to cytochrome *c* in the mixing dead time for all three mutants. This suggests that these mutants primarily exist in an open conformation in their NADPH-free forms, and in this way differ from NADPH-free WT nNOSred in having a higher K_{eq}(A) setpoint under this circumstance. These traces also show that subsequent electron transfer out of each mutant is faster than for WT nNOSred under the NADPH-free condition. Despite these differences, bound NADPH still significantly slowed electron flux out of the three fully reduced nNOSred mutants in a manner similar to that seen for WT nNOSred. In addition, bound NADPH appeared to shift the conformational distributions of the mutants towards a greater population of closed conformers (Figures 7D, 7F and 7H).

Kinetic modelling study

To understand more fully how the charge-pairing residues impact the conformational equilibrium parameters, we computer simulated the experimental kinetic traces for each NADPH-bound enzyme in Figure 6, according to a four-state kinetic model that links the rates of nNOSred conformational motions and interflavin electron transfer to the electron flux to cytochrome *c* [43] (Figure 3). We incorporated our estimated K_{eq}(A) setpoint measures and then used an iterative method to find allowable rate values for interflavin electron transfer and FMN domain conformational transitions that ultimately give a best fit of the experimental kinetic traces and of the times required to complete transfer of the first electron equivalent as indicated in Figure 6. We have used this approach previously to derive estimates of the conformational and interflavin electron transfer rate parameters for WT nNOSred and eNOSred [43]. In the present study, we were able to closely fit the experimental traces for WT nNOSred and all of the mutants except for the triple mutant (Supplementary Figure S3 at http://www.biochemj.org/bj/450/bj4500607add.htm). Table 2 reports the best-fit rates that we derived for the interflavin electron transfer and the FMN domain conformational motions. The rates derived for WT nNOSred are close to those reported in the original study [43]. In comparison, the simulations of the mutant kinetic traces indicate that they all must have higher interflavin electron transfer rates and higher rates of FMN domain conformational transitions relative to WT, in order to support their observed rates of electron flux to cytochrome *c*.

DISCUSSION

Interdomain charge-pairing interactions are among several structural features thought to govern electron flux through NOS enzymes [8,47]. In the present study, we investigated three residues that form charge-pairing interactions at the NADPH/FAD–FMN domain interface (Glu^{762}, Glu^{816} and Glu^{819}) that were previously shown to help govern electron flux through the CaM-free nNOS [38], asking whether they do so by controlling the conformational behaviour of nNOSred. We found that reversing or eliminating the negative charge at each of these residues did alter nNOSred conformational behaviours in a manner that was consistent with, and sufficient to explain, the observed changes in electron flux through the enzyme to cytochrome *c*. Thus we conclude that the charge-pairing interactions of Glu^{762}, Glu^{816} and Glu^{819}, as observed in the crystal structure [6,38], each help to retard electron flux through CaM-free nNOSred by influencing the conformational K_{eq}(A) setpoint and its associated conformational kinetic parameters.

Our modelling study indicated that eliminating the interdomain charge pairings altered both the K_{eq}(A) setpoint and the associated rates of conformational switching between the open and closed states of nNOSred. In all cases, but to varying degrees, there was a shift in the K_{eq}(A) setpoint to favour the open or FMN-deshielded form of nNOSred, which was accompanied by significantly higher rates of conformational switching (i.e. k_1 and k_{-1}). Because the mutant K_{eq}(A) setpoints all rose above 1, which is predicted to be the optimal setting for electron flux through nNOSred [43], there had to be accompanying rate increases in the conformational opening steps (k_{-1} and k_{-3}) and the conformational closing steps (k_1 and k_3) in order to satisfy the observed faster cytochrome *c* reductase activities of the mutants. Evidence leading to these conclusions is discussed below.

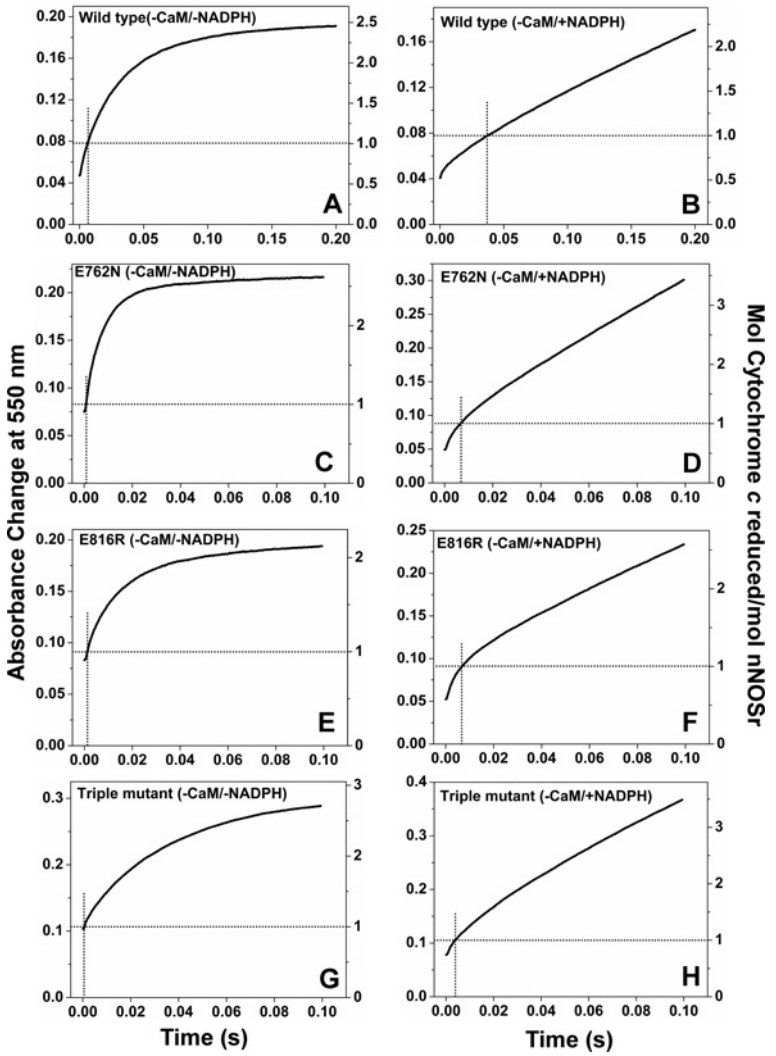

Figure 7 Effect of NADPH on the conformational equlibrium of WT nNOSred and variants

Photoreduced nNOSred proteins in the presence or absence of NADPH were mixed with a 10-fold molar excess of cytochrome *c* in a stopped-flow spectrophotometer under anaerobic conditions at 10 °C as described in the Experimental section. Kinetic traces were recorded at 550 nm during the first few electron transfers to cytochrome *c*. The absorbance change representing the transfer of the first electron equivalent from nNOSred is shown by broken lines according to the right-hand scale in each Figure. The results are representative of at least two experiments.

Impact on the K_{eq}(A) setpoint of nNOSred

Results from the experiments where the fully reduced NADPH-bound forms of nNOSred proteins were mixed with a large molar excess of cytochrome *c* (traces in Figure 6; Table 2) indicated that 55–60 % of the singly mutated proteins exist in the open state, whereas the triple mutant exists as 70 % in the open state. These percentages fall between those observed for CaM-free WT nNOSred (approximately 50 % open) and CaM-bound WT nNOSred (approximately 90 % open) when in their fully reduced NADPH-bound forms [20,21]. This relatively mild impact on the conformational equilibrium setpoint is consistent with the single charges at Glu^{762}, Glu^{816} and Glu^{819} all co-operating to stabilize the closed form of nNOSred, and with CaM causing a more extensive destabilization of the closed conformation by distinct mechanisms that override the interdomain charge-pairing stabilization. Interestingly, a given mutation's capacity to increase the K_{eq}(A) setpoint was not always well correlated with its capacity to increase electron flux through the CaM-free protein to cytochrome *c* (i.e. increase the reductase activity, see Figure 4), suggesting that other effects besides simply shifting the K_{eq}(A) setpoint are important, as discussed below.

Simulations imply an increase in conformational transition rates

Previous computer simulations of our kinetic model in Figure 3 indicated that an optimal electron flux through nNOSred to cytochrome *c* should occur at or near a K_{eq}(A) setting of 1 [8,43]. Given that the Glu^{762}, Glu^{816} and Glu^{819} mutants all have values of $K_{eq}(A)>1$, this stipulates that their conformational transition rates (k_1, k_3, k_{-1} and k_{-3}) would have to increase in order for the mutants to be capable of supporting greater electron flux to cytochrome *c* relative to WT nNOSred. Indeed, our best fits of the experimental traces for cytochrome *c* reduction by the mutant proteins indicated that the mutants should all have significantly higher conformational transition rates (1.5–4-fold) and corresponding higher rates of interflavin electron transfer (1.5–2-fold) relative to WT to support their observed faster electron flux to cytochrome *c*. These predicted increases in the

conformational transition rates are remarkable, considering that they result from reversing or neutralizing single surface charges that participate in interdomain charge pairing across a domain interface. Thus we conclude that the interdomain charge-pairing interactions of Glu^{762}, Glu^{816} and Glu^{819} have a combined function: they lower the K_{eq}(A) setpoint of CaM-free nNOSred, and also retard the associated conformational transition rates between its open and closed forms, thereby restricting electron flux through the enzyme.

NADP(H)-induced conformational effects remain intact

The results of the present study indicate that NADPH binding to the fully reduced WT nNOSred causes little or no shift in its conformational equilibrium setpoint toward the closed form. This conclusion differs markedly from what we and other groups have reported previously, namely that NADPH has a strong effect in stabilizing the closed conformation [7,19,24,25]. However, these preivous studies used a different experimental approach in which cytochrome *c* was rapidly mixed with a 5–10-fold molar excess of reduced NOSred enzyme. Because the cytochrome *c* concentration is rate limiting in this circumstance, the reaction of the open nNOSred conformer does not finish in the mixing dead time as it does for the reactions depicted in Figures 6 and 7, but instead evolves over the first 50–100 ms. If the open and closed nNOSred species could not interconvert, or could only interconvert slowly relative to this timeframe, then this method could report on the K_{eq}(A) setpoint and the effect of bound NADPH, because under these circumstances the measured exponential rates would be directly proportional to the concentration of open nNOSred that is present at the time of mixing. This has, in fact, been the historical assumption. However, our previous studies [20,43] clearly show that these kinetic conditions do not exist for nNOSred. Specifically, the 50–100 ms timeframes provide ample time for nNOSred to interconvert between its conformers (i.e. an opening of the closed reduced form, and the closing of the reacted open form), and even allow some time for interflavin electron transfer to regenerate some FMNhq (FMN hydroquinone) from FMNsq. This means that kinetic traces collected under this former experimental condition actually represent a blend of rates that reflect the amount of open reactive nNOSred that is present at the time of mixing, plus an evolving and complex combination of rates for other processes that generate more of the open reactive form of nNOSred during the timeframe of measurement. This complexity means that the former experimental method cannot determine how bound NADPH may impact the K_{eq}(A) setpoint of nNOSred, and also means that the previous conclusions regarding a strong NADPH effect on K_{eq}A setpoint need to be reconsidered. In the present study, NADPH had little effect on K_{eq}(A) in WT nNOSred, and only appeared to stabilize the closed conformation to a modest extent in the three mutant enzymes that we examined.

On the other hand, we found that bound NADPH exerted a strong repressive effect on electron flux out of the fully reduced WT nNOSred and the mutant enzymes. Bound NADPH greatly repressed the rates of the first and subsequent electron transfer events out of the enzyme in all cases (see Figure 7). This suggests that bound NADPH predominantly exerts a kinetic effect. On the basis of our findings, we speculate that bound NADPH must retard the switching rates between the open and closed nNOSred conformers [without altering the K_{eq}(A) setpoint much], and/or retard the rate of interflavin electron transfer. This shifts the current paradigm regarding how NADPH is thought to influence nNOSred conformational aspects related to electron flux, away from a predominant effect on K_{eq}(A) setpoint and towards an effect on the conformational switching kinetics. These possibilities should now be explored. For the present study, we can conclude that the interdomain charge-pairing interactions of Glu^{762}, Glu^{816} and Glu^{819} do not significantly influence the conformational response of nNOSred to bound NADPH. This makes sense, given their remote location from the nNOSred structural features that sense bound NADPH [24,25] and help transduce its effects [9].

Faster electron import and flavin reduction

The CaM-free mutants all had higher rates of NADPH-dependent flavin reduction compared with WT nNOSred (Table 1). This implies that, much like CaM, the mutations eased the kinetic repression on electron import that is normally present in CaM-free nNOS [22,45]. Rate increases in the mutants were clearly evident in the first and second phases of flavin reduction, which would encompass the first hydride transfer from NADPH to FAD and the interflavin ($FADH_2$ to FMN) electron transfer steps [7,19,24,40,44], and also include a portion of subsequent steps, including $NADP^+$ dissociation, binding of a second molecule of NADPH, a second hydride transfer to FAD and additional interflavin electron transfers. It is interesting to consider how the charge-pairing interactions of these residues, which are located in the FMN domain, might 'remotely' retard electron import from NADPH into nNOSred. Adak et al. [41] first showed that the kinetic inhibition on electron import into CaM-free nNOS requires an intact FMN domain, and this was subsequently confirmed in studies with nNOS constructs with deleted FMN domains [44,48,49]. One possible explanation that is most consistent with the results from the present study comes from work by Welland and Daff [50], who proposed that the hydride transfer from NADPH to FAD requires that nNOSred be in its open conformation. They suggested that the first (fastest) phase of flavin reduction involves the portion of enzyme molecules that are already in the open conformation, whereas the second phase of flavin reduction involved the remaining enzyme molecules that are in the closed conformation and reflected the rate by which they transition to the open state. Thus their model has the open state supporting two distinct steps; namely, facilitating hydride transfer from NADPH to FAD on one hand, and enhancing electron transfer out of the reduced nNOSred to cytochrome *c* on the other hand [8,47]. Accordingly, these concepts suggest that the higher flavin reduction rates we observed in our mutants reflect their higher K_{eq}(A) setpoints, and perhaps more importantly reflect their higher rates of conformational switching between the closed and open states. A higher rate of conformational switching would also facilitate the interflavin electron transfer between FAD and FMN, and thus further explain why the mutants have higher second phase rates of flavin reduction. Although consistent with the results of the present study, definitive testing of these concepts will require a more direct measure of the conformational switching rates, which is probably achievable only at the single molecule level. In any case, the results of the present study highlight how interdomain charge-pairing interactions can regulate both electron import and export in nNOSred.

Increased O_2 reactivity of the flavins

Some of the single mutants, and particularly the triple mutant, showed increased reactivity with O_2 that in some cases was associated with a kinetic destabilization of the FMNsq. This may reflect an increased access of dioxygen and/or disruption of

protective mechanisms that NOS and other dual-flavin enzymes use to shield their reduced flavins from auto-oxidation. Such changes diminish the fidelity of electron transfer through the mutant reductase domains to cytochrome *c* or to the NOS haem domain, and result in greater production of reduced oxygen species.

Summary and concluding remarks

Our findings from the present study support a model where electron flux through nNOSred is governed primarily by protein conformational aspects. They suggest that three electronegative residues on the FMN domain of nNOSred (Glu^{762}, Glu^{816} and Glu^{819}) that participate in charge-pairing interactions at the NADPH/FAD and FMN domain interface [38] help to stabilize fully reduced nNOSred in a closed or FMN-shielded conformational state, and also help to retard the switching rates between the open and closed conformations. Their combined influence helps to repress NADPH-dependent electron flux through nNOSred when it is in the CaM-free state. CaM binding largely overrides the influence of the charge-pairing interactions and allows faster electron flux through nNOSred.

Given that rates of electron loading and electron flux are improved in the mutant nNOSred proteins, one might question why the interdomain charge-pairing interactions involving Glu^{762}, Glu^{816} and Glu^{819} were maintained in nNOS during evolution. One obvious reason is they seem to retard flavin auto-oxidation reactions, and so help to minimize production of reactive oxygen species during catalysis. Moreover the electronegative residues might play an additional role in the full-length nNOS to help the FMN domain achieve a productive electrostatic interaction with the NOSoxy domain for electron transfer to the haem, as indicated by structural analysis and computer docking studies [39]. In this way, the charge-pairing interactions may allow a sufficient and coupled electron flux while still enabling the FMN domain to interact with both its electron-donating and electron-accepting partner domains during catalysis.

AUTHOR CONTRIBUTION

Mohammad Mahfuzul Haque and Mekki Bayachou designed and performed the experiments and analysed the data. Mohammed Fadlalla performed the steady state assays. Deborah Durra purified the proteins. Mohammad Mahfuzul Haque and Mekki Bayachou drafted the paper. Dennis Stuehr designed the research, analysed the data and wrote the final paper.

ACKNOWLEDGEMENT

We thank Dr Jesus Tejero for his help in making the crystal structure Figure.

FUNDING

This work was supported by the National Institutes of Health [grant numbers GM51491 and HL58883 (to D.J.S.)]

REFERENCES

1 Knott, A. B. and Bossy-Wetzel, E. (2009) Nitric oxide in health and disease of the nervous system. Antioxid. Redox. Signal. **11**, 541–554
2 Furchgott, R. F. (1999) Endothelium-derived relaxing factor: discovery, early studies, and identification as nitric oxide. Biosci. Rep. **19**, 235–251
3 Stuehr, D. J. (1999) Mammalian nitric oxide synthases. Biochim. Biophys. Acta **1411**, 217–230
4 Li, H. and Poulos, T. L. (2005) Structure-function studies on nitric oxide synthases. J. Inorg. Biochem. **99**, 293–305
5 Crane, B. R., Arvai, A. S., Ghosh, D. K., Wu, C., Getzoff, E. D., Stuehr, D. J. and Tainer, J. A. (1998) Structure of nitric oxide synthase oxygenase dimer with pterin and substrate. Science **279**, 2121–2126
6 Garcin, E. D., Bruns, C. M., Lloyd, S. J., Hosfield, D. J., Tiso, M., Gachhui, R., Stuehr, D. J., Tainer, J. A. and Getzoff, E. D. (2004) Structural basis for isozyme-specific regulation of electron transfer in nitric-oxide synthase. J. Biol. Chem. **279**, 37918–37927
7 Guan, Z. W., Haque, M. M., Wei, C. C., Garcin, E. D., Getzoff, E. D. and Stuehr, D. J. (2010) Lys842 in neuronal nitric-oxide synthase enables the autoinhibitory insert to antagonize calmodulin binding, increase FMN shielding, and suppress interflavin electron transfer. J. Biol. Chem. **285**, 3064–3075
8 Stuehr, D. J., Tejero, J. and Haque, M. M. (2009) Structural and mechanistic aspects of flavoproteins: electron transfer through the nitric oxide synthase flavoprotein domain. FEBS J. **276**, 3959–3974
9 Tiso, M., Tejero, J., Panda, K., Aulak, K. S. and Stuehr, D. J. (2007) Versatile regulation of neuronal nitric oxide synthase by specific regions of its C-terminal tail. Biochemistry **46**, 14418–14428
10 Eschenbrenner, M., Coves, J. and Fontecave, M. (1995) The flavin reductase activity of the flavoprotein component of sulfite reductase from *Escherichia coli*. A new model for the protein structure. J. Biol. Chem. **270**, 20550–20555
11 Finn, R. D., Basran, J., Roitel, O., Wolf, C. R., Munro, A. W., Paine, M. J. and Scrutton, N. S. (2003) Determination of the redox potentials and electron transfer properties of the FAD- and FMN-binding domains of the human oxidoreductase NR1. Eur. J. Biochem. **270**, 1164–1175
12 Munro, A. W., Leys, D. G., McLean, K. J., Marshall, K. R., Ost, T. W., Daff, S., Miles, C. S., Chapman, S. K., Lysek, D. A., Moser, C. C. et al. (2002) P450 BM3: the very model of a modern flavocytochrome. Trends Biochem. Sci. **27**, 250–257
13 Wolthers, K. R. and Scrutton, N. S. (2007) Protein interactions in the human methionine synthase-methionine synthase reductase complex and implications for the mechanism of enzyme reactivation. Biochemistry **46**, 6696–6709
14 Zeghouf, M., Fontecave, M. and Coves, J. (2000) A simplifed functional version of the *Escherichia coli* sulfite reductase. J. Biol. Chem. **275**, 37651–37656
15 Zhang, J., Martasek, P., Paschke, R., Shea, T., Masters, B. S. S. and Kim, J. J. (2001) Crystal structure of the FAD/NADPH-binding domain of rat neuronal nitric-oxide synthase. Comparisons with NADPH-cytochrome P450 oxidoreductase. J. Biol. Chem. **276**, 37506–37513
16 Siddhanta, U., Presta, A., Fan, B., Wolan, D., Rousseau, D. L. and Stuehr, D. J. (1998) Domain swapping in inducible nitric-oxide synthase. Electron transfer occurs between flavin and heme groups located on adjacent subunits in the dimer. J. Biol. Chem. **273**, 18950–18958
17 Wei, C. C., Crane, B. R. and Stuehr, D. J. (2003) Tetrahydrobiopterin radical enzymology. Chem. Rev. **103**, 2365–2383
18 Klatt, P., Heinzel, B., John, M., Kastner, M., Bohme, E. and Mayer, B. (1992) Ca^{2+}/calmodulin-dependent cytochrome *c* reductase activity of brain nitric oxide synthase. J. Biol. Chem. **267**, 11374–11378
19 Craig, D. H., Chapman, S. K. and Daff, S. (2002) Calmodulin activates electron transfer through neuronal nitric-oxide synthase reductase domain by releasing an NADPH-dependent conformational lock. J. Biol. Chem. **277**, 33987–33994
20 Ilagan, R. P., Tiso, M., Konas, D. W., Hemann, C., Durra, D., Hille, R. and Stuehr, D. J. (2008) Differences in a conformational equilibrium distinguish catalysis by the endothelial and neuronal nitric-oxide synthase flavoproteins. J. Biol. Chem. **283**, 19603–19615
21 Ilagan, R. P., Tejero, J., Aulak, K. S., Ray, S. S., Hemann, C., Wang, Z. Q., Gangoda, M., Zweier, J. L. and Stuehr, D. J. (2009) Regulation of FMN subdomain interactions and function in neuronal nitric oxide synthase. Biochemistry **48**, 3864–3876
22 Welland, A., Garnaud, P. E., Kitamura, M., Miles, C. S. and Daff, S. (2008) Importance of the domain-domain interface to the catalytic action of the NO synthase reductase domain. Biochemistry **47**, 9771–9780
23 Feng, C. (2012) Mechanism of nitric oxide synthase regulation: electron transfer and interdomain interactions. Coord. Chem. Rev. **256**, 393–411
24 Konas, D. W., Zhu, K., Sharma, M., Aulak, K. S., Brudvig, G. W. and Stuehr, D. J. (2004) The FAD-shielding residue Phe1395 regulates neuronal nitric-oxide synthase catalysis by controlling $NADP^+$ affinity and a conformational equilibrium within the flavoprotein domain. J. Biol. Chem. **279**, 35412–35425
25 Tiso, M., Konas, D. W., Panda, K., Garcin, E. D., Sharma, M., Getzoff, E. D. and Stuehr, D. J. (2005) C-terminal tail residue Arg1400 enables NADPH to regulate electron transfer in neuronal nitric-oxide synthase. J. Biol. Chem. **280**, 39208–39219
26 Ghosh, D. K., Ray, K., Rogers, A. J., Nahm, N. J. and Salerno, J. C. (2012) FMN fluorescence in inducible NOS constructs reveals a series of conformational states involved in the reductase catalytic cycle. FEBS J. **279**, 1306–1317

27 Daff, S., Sagami, I. and Shimizu, T. (1999) The 42-amino acid insert in the FMN domain of neuronal nitric-oxide synthase exerts control over Ca^{2+} /calmodulin-dependent electron transfer. J. Biol. Chem. **274**, 30589–30595

28 Roman, L. J. and Masters, B. S. (2006) Electron transfer by neuronal nitric oxide synthase is regulated by concerted interaction of calmodulin and two intrinsic regulatory elements. J. Biol. Chem. **281**, 23111–23118

29 Lane, P. and Gross, S. S. (2002) Disabling a C-terminal autoinhibitory control element in endothelial nitric-oxide synthase by phosphorylation provides a molecular explanation for activation of vascular NO synthesis by diverse physiological stimuli. J. Biol. Chem. **277**, 19087–19094

30 Roman, L. J., Miller, R. T., de La Garza, M. A., Kim, J. J. and Masters, B. S. S. (2000) The C terminus of mouse macrophage inducible nitric-oxide synthase attenuates electron flow through the flavin domain. J. Biol. Chem. **275**, 21914–21919

31 Adak, S., Santolini, J., Tikunova, S., Wang, Q., Johnson, J. D. and Stuehr, D. J. (2001) Neuronal nitric-oxide synthase mutant (Ser-1412→Asp) demonstrates surprising connections between heme reduction, NO complex formation, and catalysis. J. Biol. Chem. **276**, 1244–1252

32 Butt, E., Bernhardt, M., Smolenski, A., Kotsonis, P., Frohlich, L. G., Sickmann, A., Meyer, H. E., Lohmann, S. M. and Schmidt, H. H. (2000) Endothelial nitric-oxide synthase (type III) is activated and becomes calcium independent upon phosphorylation by cyclic nucleotide-dependent protein kinases. J. Biol. Chem. **275**, 5179–5187

33 Dimmeler, S., Fleming, I., Fisslthaler, B., Hermann, C., Busse, R. and Zeiher, A. M. (1999) Activation of nitric oxide synthase in endothelial cells by Akt-dependent phosphorylation. Nature **399**, 601–605

34 Knudsen, G. M., Nishida, C. R., Mooney, S. D. and Ortiz de Montellano, P. R. (2003) Nitric-oxide synthase (NOS) reductase domain models suggest a new control element in endothelial NOS that attenuates calmodulin-dependent activity. J. Biol. Chem. **278**, 31814–31824

35 Haque, M. M., Panda, K., Tejero, J., Aulak, K. S., Fadlalla, M. A., Mustovich, A. T. and Stuehr, D. J. (2007) A connecting hinge represses the activity of endothelial nitric oxide synthase. Proc. Natl. Acad. Sci. U.S.A. **104**, 9254–9259

36 Adak, S., Sharma, M., Meade, A. L. and Stuehr, D. J. (2002) A conserved flavin-shielding residue regulates NO synthase electron transfer and nicotinamide coenzyme specificity. Proc. Natl. Acad. Sci. U.S.A. **99**, 13516–13521

37 Haque, M. M., Fadlalla, M., Wang, Z. Q., Ray, S. S., Panda, K. and Stuehr, D. J. (2009) Neutralizing a surface charge on the FMN subdomain increases the activity of neuronal nitric-oxide synthase by enhancing the oxygen reactivity of the enzyme heme-nitric oxide complex. J. Biol. Chem. **284**, 19237–19247

38 Panda, K., Haque, M. M., Garcin-Hosfield, E. D., Durra, D., Getzoff, E. D. and Stuehr, D. J. (2006) Surface charge interactions of the FMN module govern catalysis by nitric-oxide synthase. J. Biol. Chem. **281**, 36819–36827

39 Tejero, J., Hannibal, L., Mustovich, A. and Stuehr, D. J. (2010) Surface charges and regulation of FMN to heme electron transfer in nitric-oxide synthase. J. Biol. Chem. **285**, 27232–27240

40 Matsuda, H. and Iyanagi, T. (1999) Calmodulin activates intramolecular electron transfer between the two flavins of neuronal nitric oxide synthase flavin domain. Biochim. Biophys. Acta **1473**, 345–355

41 Adak, S., Ghosh, S., Abu-Soud, H. M. and Stuehr, D. J. (1999) Role of reductase domain cluster 1 acidic residues in neuronal nitric-oxide synthase. Characterization of the FMN-FREE enzyme. J. Biol. Chem. **274**, 22313–22320

42 Mendes, P. (1993) GEPASI: a software package for modelling the dynamics, steady states and control of biochemical and other systems. Comput. Appl. Biosci. **9**, 563–571

43 Haque, M. M., Kenney, C., Tejero, J. and Stuehr, D. J. (2011) A kinetic model linking protein conformational motions, interflavin electron transfer and electron flux through a dual-flavin enzyme-simulating the reductase activity of the endothelial and neuronal nitric oxide synthase flavoprotein domains. FEBS J. **278**, 4055–4069

44 Guan, Z. W. and Iyanagi, T. (2003) Electron transfer is activated by calmodulin in the flavin domain of human neuronal nitric oxide synthase. Arch. Biochem. Biophys. **412**, 65–76

45 Gachhui, R., Presta, A., Bentley, D. F., Abu-Soud, H. M., McArthur, R., Brudvig, G., Ghosh, D. K. and Stuehr, D. J. (1996) Characterization of the reductase domain of rat neuronal nitric oxide synthase generated in the methylotrophic yeast *Pichia pastoris*. Calmodulin response is complete within the reductase domain itself. J. Biol. Chem. **271**, 20594–20602

46 Knight, K. and Scrutton, N. S. (2002) Stopped-flow kinetic studies of electron transfer in the reductase domain of neuronal nitric oxide synthase: re-evaluation of the kinetic mechanism reveals new enzyme intermediates and variation with cytochrome P450 reductase. Biochem. J. **367**, 19–30

47 Daff, S. (2010) NO synthase: structures and mechanisms. Nitric Oxide **23**, 1–11

48 Dunford, A. J., Marshall, K. R., Munro, A. W. and Scrutton, N. S. (2004) Thermodynamic and kinetic analysis of the isolated FAD domain of rat neuronal nitric oxide synthase altered in the region of the FAD shielding residue Phe1395. Eur. J. Biochem. **271**, 2548–2560

49 Konas, D. W., Takaya, N., Sharma, M. and Stuehr, D. J. (2006) Role of Asp^{1393} in catalysis, flavin reduction, NADP(H) binding, FAD thermodynamics, and regulation of the nNOS flavoprotein. Biochemistry **45**, 12596–12609

50 Welland, A. and Daff, S. (2010) Conformation-dependent hydride transfer in neuronal nitric oxide synthase reductase domain. FEBS J. **277**, 3833–3843